


# Comparative Evaluation of Superb Microvascular Imaging and Dynamic Contrast-Enhanced Magnetic Resonance Imaging in Differentiating Benign and Malignant Breast Masses

Ahmet Yasin Yitik, MD , Nuran Sabir, MD , Sevda Yilmaz, MD 

 Supplemental material online at [ultrasoundmed.org](https://ultrasoundmed.org)

Received November 5, 2024, from the Department of Radiology, Pamukkale University Medical Faculty Hospital, Denizli, Turkey (A.Y.Y., N.S.); and Department of General Surgery, Pamukkale University Medical Faculty Hospital, Denizli, Turkey (S.Y.). Manuscript accepted for publication February 2, 2025.

The authors declare that there are no conflicts of interest regarding the publication of this manuscript.

This study has been accepted for a presentation at the European Society of Breast Imaging (EUSOBI) 2024 Annual Scientific Meeting.

Address correspondence to Ahmet Yasin Yitik, Department of Radiology, Pamukkale University Medical Faculty Hospital, Denizli, Turkey.

E-mail: [ahmetyasinyitik@gmail.com](mailto:ahmetyasinyitik@gmail.com)

## Abbreviations

AUC, area under the curve; CDUS, color Doppler ultrasonography; DCE, dynamic contrast-enhanced; DWI, diffusion-weighted Imaging; MIP, maximum intensity projection; MRI, magnetic resonance imaging; NPV, negative predictive value; PCAS, Picture Archive Communication System; PDUS, power Doppler ultrasonography; PPV, positive predictive value; ROI, region of interest; SMI, superb microvascular imaging; STIR, short tau inversion recovery; US, ultrasonography; VI, vascular index; WI, Washout Index

doi:10.1002/jum.16664

This is an open access article under the terms of the [Creative Commons Attribution-NonCommercial-NoDerivs](https://creativecommons.org/licenses/by-nc/4.0/) License, which permits use and distribution in any medium, provided the original work is properly cited, the use is non-commercial and no modifications or adaptations are made.

**Objectives**—Our study aims to compare the diagnostic performance of superb microvascular imaging (SMI) and dynamic contrast-enhanced magnetic resonance imaging (MRI) in differentiating benign from malignant breast masses, using histopathological findings as the reference standard.

**Methods**—This prospective study was conducted from April 2022 to March 2024. A total of 112 breast lesions from 110 patients were evaluated using gray-scale ultrasonography, SMI, and dynamic contrast-enhanced MRI. The vascular index (VI) obtained during SMI examination and kinetic curve patterns from MRI were analyzed.

**Results**—Histopathological analysis revealed 62 benign and 50 malignant lesions. The VI showed a statistically significant difference between benign and malignant lesions, with a mean VI of  $5.12 \pm 4.66$  in benign masses and  $10.13 \pm 5.48$  in malignant masses ( $P < .001$ ). The ROC analysis demonstrated an AUC of 0.79 for SMI with a VI cut-off value of 4.15, yielding a sensitivity of 92%, specificity of 60%, and accuracy of 74%. A statistically significant correlation was found between VI values and MRI contrast enhancement kinetic curve types ( $P < .05$ ). MRI demonstrated superior diagnostic performance, with an AUC of 0.89 and sensitivity, specificity, and accuracy of 98, 80.65, and 88.39%, respectively.

**Conclusions**—SMI, when used in conjunction with conventional ultrasonography and MRI, provides significant diagnostic value in differentiating benign from malignant breast masses. The study supports the potential integration of SMI into routine breast cancer diagnostic workflows, particularly in settings where MRI is less accessible.

**Key Words**—breast cancer; breast imaging; magnetic resonance imaging; superb microvascular imaging; vascular index

## Introduction

Breast cancer is the most prevalent cancer among women globally, accounting for approximately one-fifth of all cancer cases. According to GLOBOCAN 2022 data, breast cancer is the second leading cause of cancer-related mortality among

women, following lung cancer.<sup>1</sup> The incidence of breast cancer has been steadily increasing, with an annual rise of approximately 0.4%.<sup>2</sup> The 5-year survival rates for breast cancer vary significantly depending on the stage at diagnosis: 99% for localized cases, 86% for regional spread, and 31% for distant metastases. These figures underscore the critical importance of early detection in breast cancer management, as diagnosing the disease at an early stage not only improves survival outcomes but also allows for less invasive treatment options.<sup>3</sup> Early detection is most important in breast cancer management, as diagnosing the disease at an early stage can lead to less invasive treatments and significantly improve patient survival rates.

In the screening and diagnosis of breast cancer, mammography, and ultrasonography (US) are the primary modalities employed. Breast cancer detection sensitivity varies among imaging modalities: 25–58% for mammography, 33–52% for ultrasound, 48–67% for the combination of mammography and ultrasound, and 71–100% for magnetic resonance imaging (MRI). Specificity ranges from 93 to 100% for mammography, 91 to 98% for ultrasound, 89 to 98% for the combined approach, and 81 to 98% for MRI.<sup>4</sup> However, despite their widespread use, these methods often fall short of the desired sensitivity and specificity. This limitation has led to the increased utilization of MRI as a supplementary tool, particularly in complex cases where conventional methods may not provide conclusive results.<sup>5</sup> Tumor growth, local invasion, and distant metastasis are significantly influenced by neovascularization, the formation of new blood vessels, a process that plays a crucial role in the pathophysiology of cancer. The degree of neovascularization is directly proportional to the metastatic potential of the lesion and inversely proportional to the patient's prognosis.<sup>6</sup>

Current imaging techniques to evaluate neovascularization include color Doppler ultrasonography (CDUS), power Doppler ultrasonography (PDUS), contrast-enhanced US, contrast-enhanced mammography, and dynamic contrast-enhanced (-DCE) MRI.<sup>5,7–10</sup> Conventional Doppler methods often struggle to visualize microvascular structures due to the slow blood flow within these small vessels. To address this challenge, superb microvascular imaging (SMI) has been developed as a novel Doppler

technique. SMI enhances the visualization of microvascular structures and provides a quantitative assessment of vascularization through the vascular index (VI) without the limitations imposed by conventional Doppler techniques.<sup>11</sup> VI measures the ratio of colored pixels to the total number of pixels within a defined region of interest (ROI) and is calculated automatically by software integrated into the scanner. Thus, as it represents a percentage, it is dimensionless and does not have any units.<sup>12</sup>

DCE MRI is a critical tool in diagnostic imaging, particularly for lesion characterization. The enhancement kinetic curve patterns observed during DCE imaging are classified into three primary types: persistent, plateau, and washout. A persistent pattern, characterized by a continuous increase in signal intensity over time, is generally associated with benign pathology. The plateau pattern, which exhibits a rapid initial rise in signal intensity followed by stabilization, is commonly linked to lesions of intermediate or uncertain significance. In contrast, the washout pattern, defined by a sharp initial increase in signal intensity followed by a subsequent decline, is strongly indicative of malignancy. These kinetic curves are quantified using time-intensity values, which represent changes in signal intensity (measured in arbitrary units) over time (typically in seconds or minutes). The interpretation of these patterns and their corresponding values provides valuable diagnostic insights, facilitating the differentiation between benign and malignant lesions.<sup>13</sup>

The objective of this study is to compare the diagnostic performance of SMI and DCE breast MRI in differentiating benign from malignant breast masses, using histopathological results as the reference standard. By integrating the VI obtained through SMI with findings from grayscale US and dynamic MRI, this study aims to evaluate the effectiveness of these combined imaging modalities in accurately diagnosing breast masses.

## Materials and Methods

### Study Population

This prospective study was conducted at Pamukkale University, Faculty of Medicine Hospital, Denizli, Türkiye from April 2022 to March 2024, following

approval from the institutional review board. Informed consent was obtained from all participants in compliance with the Declaration of Helsinki. Patients presenting with complaints of breast masses were included. A total of 171 patients who agreed to participate in the study were included. Sixty-one patients were excluded which are shown on flow chart (Figure 1). Two patients had two lesions, and the final population was 110 patients, 112 lesions.

### US and SMI Examination

The patients underwent grayscale US and SMI which were performed using a Toshiba Aplio 500 ultrasound machine (Canon Medical Systems Corporation, Tokyo, Japan) with a high-frequency (7–14 MHz) linear probe. Initially, a comprehensive scan of the breasts was conducted using grayscale ultrasound. Upon detecting a lesion, the morphologic features of the breast lesions which included lesion shape (oval-round, irregular), margin characteristics (circumscribed, not-circumscribed), and orientation (parallel, not parallel), echo pattern (isoechoic—hyperechoic, hypoechoic), and posterior features (no shadowing, shadowing) were documented. The optimal tumor imaging in the maximal plane was chosen for further analysis. The maximal diameter of the lesion and its depth (the greatest vertical distance from the skin surface to the base of the mass) were

noted. Subsequently, SMI was utilized to assess the vascularity within and surrounding the lesions. A minimum of two orthogonal planes showing the areas of richest vasculature for each lesion were acquired as video clips. For SMI, 10 to 15-second cine clips of both sagittal and transverse planes were captured for all subjects which were sent to PACS (Picture Archive Communication System). Free-hand ROI was drawn to encompass the entire lesion, and VI was automatically calculated by the system. Each lesion was measured three times independently, and the mean value of these three measurements was calculated and used for the analysis. For SMI settings, the color velocity scale was set between 1.5 and 2.5 cm/s, mechanical index 1.6, and frame rates were maintained above 50 Hz. Gain settings were optimized individually for each participant. During the examinations, patients were instructed to breathe quietly, and minimal pressure was applied to avoid vessel collapse (Figure 2).

### MRI Examination

All MRI examinations were performed utilizing an eight-channel breast coil on a 1.5-T MRI device (Signa Excite HD, General Electric Healthcare, Milwaukee, WI, USA), with patients in the prone position. Gadolinium-based contrast agent (Gadoterate Meglumine—Clariscan™) was injected intravenously

**Figure 1.** Flowchart of eligible patients.

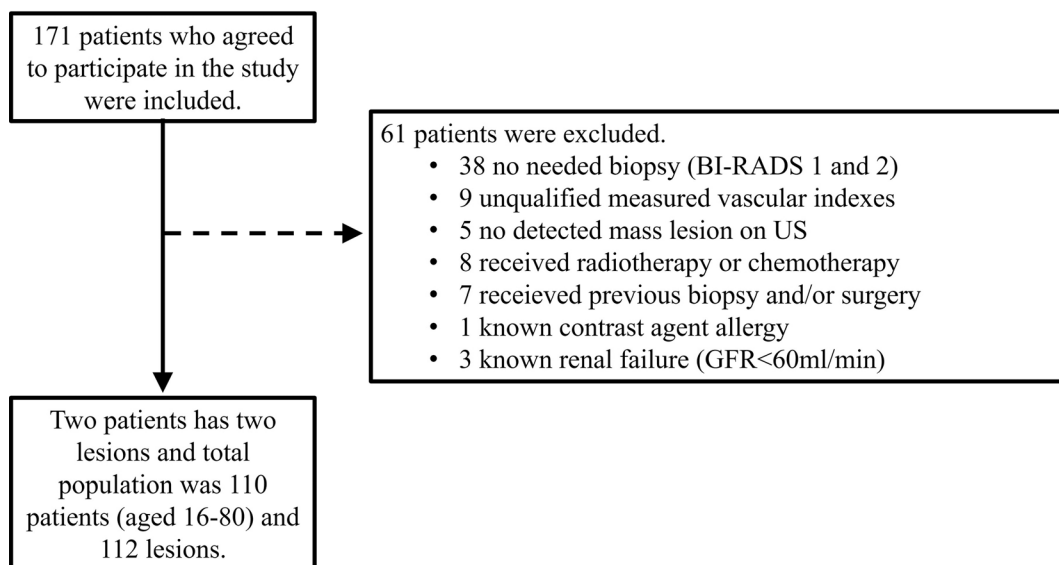
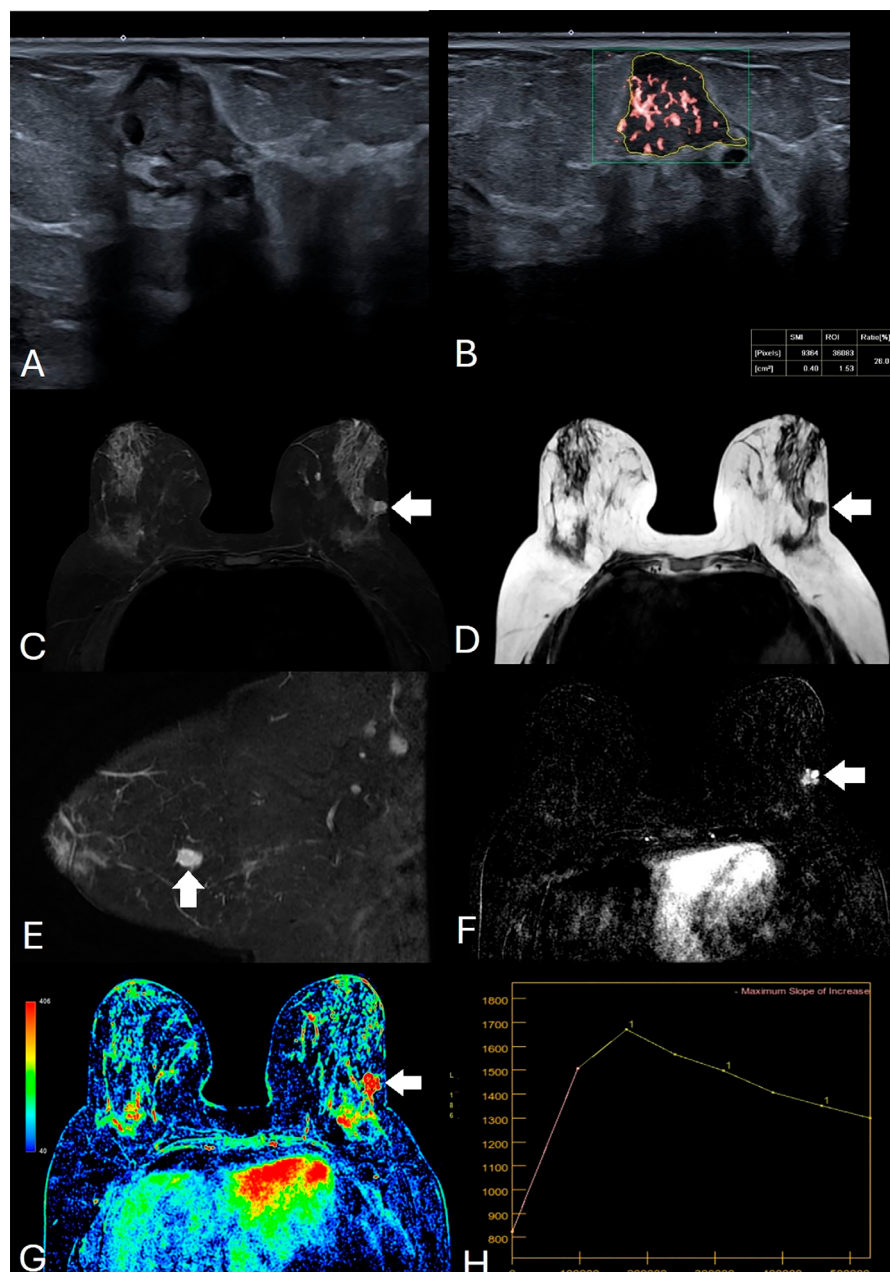


**Figure 2.** A 68-year-old female patient underwent US examination that revealed a non-circumscribed shaped, irregular margin, not-parallel oriented, hypoechoic mass lesion without posterior acoustic shadowing (**A**). On SMI (**B**), vascular structures within a freehand drawn ROI and the automatically measured VI value (VI: 28.2) by the device were observed. Magnetic resonance imaging demonstrated a hyperintense lesion on axial fat-suppressed T2WI (**C**), homogeneously enhancing on axial postcontrast sequence (**D**), hyperintense on sagittal STIR (**E**), and contrast-enhanced on sagittal postcontrast subtraction images (**F**), with a type 3 kinetic enhancement curve observed on the dynamic series (**G, H**). The mass lesion was irregularly shaped with spiculated borders (white arrows). Additionally, left axillary lymphadenopathy was observed on axial fat-suppressed T2WI, contrast-enhanced, and dynamic images. The histopathological diagnosis was confirmed as invasive ductal carcinoma.





at a dose of 0.1–0.2 mmol/kg as a single bolus injection using an automated syringe, delivered at a rate of 2 mL/s, followed by a 20 mL saline flush. For the dynamic imaging sequence, nine sequential scans were acquired both pre- and post-contrast agent administration, with each scan having a duration of 60 seconds and consisting of 64 single-phase scan slices. The standard MRI protocol encompasses axial fat-suppressed T2-weighted sequences, sagittal short tau inversion recovery (STIR) T2-weighted sequences, axial non-fat-suppressed T1-weighted sequences, and both axial and sagittal fat-suppressed T1-weighted DCE sequences, performed before and after the intravenous administration of a gadolinium-based contrast agent. Additionally, diffusion-weighted imaging (DWI) was conducted. Subtraction images and maximum intensity projection (MIP) images were also produced (Figure 3). The parameters of MRI are shown on the supplemental material S1. After imaging, all sequences were transferred to the device's workstation (AW VolumeShare 7, GE Medical Systems, Milwaukee, WI, USA). A ROI was selectively placed in areas exhibiting the most rapid and pronounced enhancement within the identified lesion. A time–signal intensity curve was then automatically generated. The percentage enhancement was calculated using the following formula for the Washout Index (WI):  $[(SI_{\text{post}} - SI_{\text{pre}})/SI_{\text{pre}}] \times 100$  where  $SI_{\text{pre}}$  denotes the signal intensity within the ROI on the unenhanced image, and  $SI_{\text{post}}$  represents the signal intensity within the ROI on the contrast-enhanced image. The quantitative results were categorized into three distinct enhancement curve types, aligned with qualitative evaluations: persistent enhancement, plateau, and washout. Specifically, a kinetic enhancement curve was classified as type 1 (persistent enhancement) if the percentage change exceeded 5%, type 2 (plateau) if the percentage change ranged between –5% and 5%, and type 3 (washout) if the percentage change was less than –5%.<sup>14</sup>

### Image Analysis

The findings from grayscale B-mode US and MRI were classified in accordance with the fifth edition of the American College of Radiology's BI-RADS lexicon. Grayscale US, SMI and breast MRI images were assessed by a radiologist with 25 years of experience

in breast imaging, and 5-year radiology resident in consensus, with reads between the imaging modalities occurring a minimum interval of 1 month between evaluations of US—SMI and MRI. The observers were blinded to the histopathologic outcomes of the lesions, as well as to the patient's clinical information and other imaging results.

### Statistical Analysis

Statistical analyses were conducted using IBM SPSS Statistics 29. Descriptive statistics and frequency tables were utilized to interpret findings. Continuous variables were reported as the mean  $\pm$  standard deviation and median, whereas categorical variables were described in terms of frequency and percentage. The Mann–Whitney U test evaluated the relationship between mean VI values in benign and malignant histopathological lesions. The Kruskal–Wallis test compared mean VI values with dynamic breast MRI enhancement kinetic curve patterns. ROC analysis determined the VI cut-off value. Mann Whitney U test assessed VI and morphological features in grayscale US. Sensitivity, specificity, positive predictive value (PPV), negative predictive value (NPV), and accuracy were calculated using cross tables. ROC analysis compared VI, US, and MRI with histopathological diagnoses. Percentage distributions of morphological features in US and MRI with histopathological diagnoses were examined using cross tables. Spearman's correlation coefficient analyzed the relationships between lesion size and SMG examination area, and between age and VI. The chi-square test assessed the relationship between age and histopathological diagnoses, with  $P < .05$  considered significant.

## Results

### Demographic Features

A total of 112 lesions from 110 patients (aged 16–80, mean  $47.67 \pm 13.57$ ) were included in our study, with histopathological analysis revealing 62 benign and 50 malignant lesions (Table 1). The age of the patients in the malignant group was  $53.94 \pm 11.22$  (31–80) years old, which was older than the age of  $42.61 \pm 13.26$  (16–78) years old in the benign group ( $P < .05$ ). The average depth of the lesions from the skin surface was  $8.81 \pm 5.22$  mm. The mean maximum

**Figure 3.** A 40-year-old female patient presented with a mass in the upper outer quadrant of the right breast. On grayscale ultrasonographic examination (**A**), an oval-round-shaped mass lesion with circumscribed margins, parallel oriented, hypoechoic, and without posterior acoustic shadowing was observed. On SMI (**B**), vascular structures were visualized within a freely drawn ROI, along with an automatically measured VI value of 5.3. Magnetic resonance imaging demonstrated the lesion as hyperintense on axial fat-suppressed T2WI (**C**), hypointense on axial pre-contrast T1WI (**D**), hyperintense on sagittal STIR (**E**), and homogeneously enhancing on axial contrast-enhanced subtraction images (**F**) (white arrows). In the dynamic series (**G**), the lesion exhibited a type 1 enhancement kinetic curve (**H**). Histopathological examination revealed a fibroepithelial lesion.

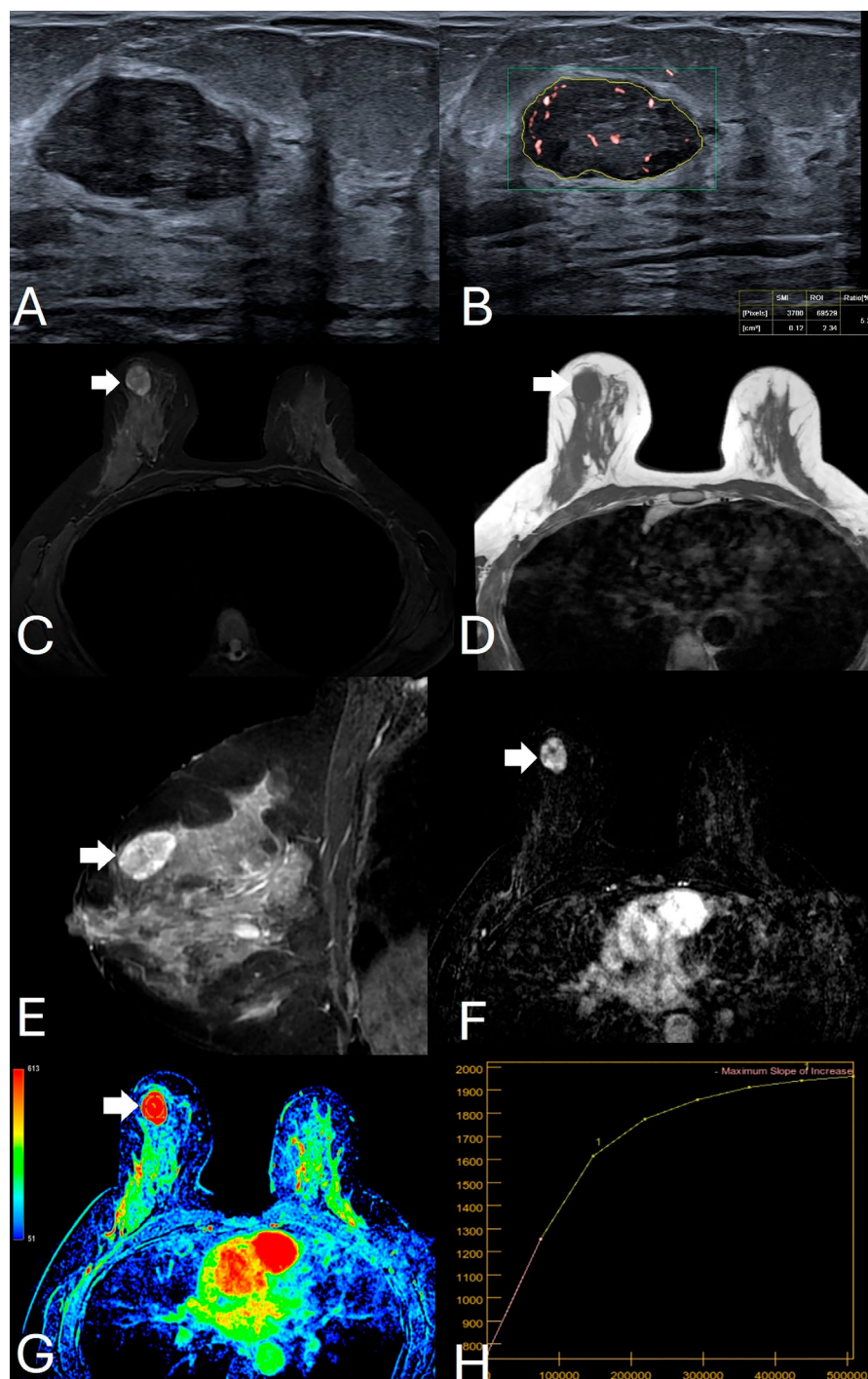


**Table 1.** The Histopathological Results of Breast Lesions

Benign Lesions	n	%	Malign Lesions	n	%
Fibroepithelial lesion	38	61.3	Invasive ductal carcinoma	41	82
Fibrocystic disease	13	21	Invasive lobular carcinoma	3	6
Intraductal papilloma	3	4.8	Ductal carcinoma in situ	1	2
Ductal epithelial hyperplasia	2	3.2	Invasive ductal carcinoma with ductal carcinoma in situ	1	2
Adenosis	1	1.6	Invasive ductal carcinoma with lobular carcinoma in situ	1	2
Benign filloides tumor	1	1.6	Invasive ductal carcinoma with tubular carcinoma	1	2
Ductal epithelial hyperplasia with adenosis	1	1.6	Invasive micropapillary carcinoma	1	2
Granulation tissue	1	1.6	Invasive mucinous carcinoma	1	2
Non-caseating granulomatous mastitis	1	1.6			
Fat necrosis	1	1.6			
Total	62	100		50	100

**Table 2.** The Relationship Between USG Morphological Features and Histopathological Results in Distinguishing Benign and Malignant Masses

US Morphological Features	Histopathological Results		Total	Chi-Square Test
	Benign	Malign	n (%)	
Lesion shape				$\chi^2 = 30.083$ <b>P &lt; .001</b>
Oval—round	56 (90.3%)	21 (42.0%)	77 (68.8%)	
Irregular	6 (9.7%)	29 (58.0%)	35 (31.3%)	
Total	62 (100.0%)	50 (100.0%)	112 (100.0%)	
Lesion margin				$\chi^2 = 37.326$ <b>P &lt; .001</b>
Circumscribed	35 (56.5%)	1 (2.0%)	36 (32.1%)	
Not circumscribed	27 (43.5%)	49 (98.0%)	76 (67.9%)	
Total	62 (100.0%)	50 (100.0%)	112 (100.0%)	
Lesion orientation				$\chi^2 = 44.544$ <b>P &lt; .001</b>
Parallel	48 (77.4%)	7 (14.0%)	55 (49.1%)	
Not parallel	14 (22.6%)	43 (86.0%)	57 (50.9%)	
Total	62 (100.0%)	50 (100.0%)	112 (100.0%)	
Lesion echo pattern				$\chi^2 = 23.912$ <b>P &lt; .001</b>
Isoechoic—hyperechoic	28 (45.2%)	2 (4.0%)	30 (26.8%)	
Hypoechoic	34 (54.8%)	48 (96.0%)	82 (73.2%)	
Total	62 (100.0%)	50 (100.0%)	112 (100.0%)	
Posterior features				$\chi^2 = 36.436$ <b>P &lt; .001</b>
No shadowing	56 (90.3%)	18 (36.0%)	74 (66.1%)	
Shadowing	6 (9.7%)	32 (64.0%)	38 (33.9%)	
Total	62 (100.0%)	50 (100.0%)	112 (100.0%)	

Bold values indicate statistically significant difference.

diameter of the lesions was  $19.38 \pm 9.67$  mm, while the mean area of the ROI measured in SMI was  $1.64 \pm 1.83$  cm<sup>2</sup>. The average VI value for all breast masses included in the study was  $7.35 \pm 5.6$ .

### Evaluation of US

Breast lesions were evaluated according to BI-RADS criteria on grayscale ultrasound, regarding lesion shape, 56 (90.3%) of the benign lesions were oval or round, while 29 (58%) of the malignant lesions had irregular shapes. When evaluating the margin

characteristics, 35 (56.5%) of benign lesions had circumscribed, while 49 (98%) of malignant lesions had non-circumscribed margins. Additionally, 43 (86%) of malignant lesions were not parallel, whereas 48 (77.4%) of benign lesions were oriented parallel. Most malignant masses (48, 96%) and benign lesions (34, 54.8%) were hypoechoic. Acoustic shadowing was present in 32 (64%) of the malignant masses. A statistically significant relationship was found between morphological features and histopathological results ( $P < .05$ ) (Table 2).

### Evaluation of Vascularity by VI

Statistically significant relationships were identified between VI values and the characteristics of lesion edges, orientation, echogenicity, and the presence of acoustic shadowing ( $P < .05$ ). However, no significant variation in VI values was noted concerning the shape of the lesions ( $P > .05$ ) (Table 3). There was a significant correlation between VI values and the histopathological results between benign and malignant masses ( $P < .05$ ). The findings indicated that VI values were higher in malignant masses compared to benign masses.

The mean VI values for benign masses were  $5.12 \pm 4.66$ , while for malignant masses, the mean was  $10.13 \pm 5.48$ . A statistically significant difference was observed between the means of benign and malignant masses ( $P < .001$ ), indicating that malignant masses tend to exhibit higher VI values compared to benign masses (Table 4).

A statistically significant correlation was found between VI values and MRI contrast enhancement kinetic curve types ( $P < .05$ ). The results showed that VI values of the masses significantly increased as the kinetic curve type approached type 3. In younger patients, benign lesions exhibited higher VI values ( $r = -0.28$ ;  $P < .05$ ), whereas the VI values of malignant lesions did not show any correlation with age ( $P > .05$ ). There was a highly significant positive correlation between the measured area of ROI and lesion sizes ( $r = 0.806$ ;  $P < .001$ ) (Table 5).

### Evaluation of MRI

Malignant masses were most frequently irregular in shape (76%) and least frequently oval (2%). Benign masses were most commonly round (46.8%), followed by oval (43.5%). Regarding margin characteristics, 50 (80.6%) of benign masses had

**Table 4.** Relationship Between Vascular Index (VI) and Histopathological Results

Histopathological Results	Mean $\pm$ SD	Median [min–max]	Mann–Whitney U
VI Benign	5.12 $\pm$ 4.66	3.35 [0–18.9]	Z = 5.286
Malign	10.13 $\pm$ 5.48	9.60 [2.5–31]	<b>P &lt; .001</b>

Bold values indicate statistically significant difference.

**Table 5.** The Relationship Between Vascular Index Values and Magnetic Resonance Imaging Contrast Enhancement Kinetic Curve Types

Contrast Enhancement Kinetic Curve	Vascular Index		Kruskal–Wallis H
	Mean $\pm$ SD	Median [min–max]	
No enhancement	1 $\pm$ 0.85	1.1 [0–1.8]	$\chi^2 = 34.119$
Type 1	5.13 $\pm$ 4.13	3.85 [0.2–18.9]	<b>P &lt; .001</b>
Type 2	8.98 $\pm$ 4.97	9.25 [0.7–15.8]	
Type 3	10.61 $\pm$ 5.96	9.9 [2.3–31]	

Bold values indicate statistically significant difference.

**Table 3.** The Relationship Between Ultrasonographic (US) Morphological Features of Benign and Malign Lesions and Vascular Index (VI) Values

US Morphological Features	Mean $\pm$ SD	Median [min–max]	Mann–Whitney U
VI			
Lesion shape			Z = 1.852
Oval—round	7.00 $\pm$ 6.16	4.80 [0–31]	P = .064
Irregular	8.13 $\pm$ 4.12	8.9 [0.3–17.9]	
Lesion margin			Z = 3.031
Circumscribed	5.30 $\pm$ 4.78	3.35 [0.2–18.9]	<b>P = .002</b>
Not circumscribed	8.32 $\pm$ 5.74	8.55 [0–31]	
Lesion orientation			Z = 3.085
Parallel	5.72 $\pm$ 4.62	4.02 [0–18.9]	<b>P = .002</b>
Not parallel	8.93 $\pm$ 6.05	9.1 [0.5–31]	
Lesion echo pattern			Z = 2.714
Isoechoic—hyperechoic	5.21 $\pm$ 4.59	3.25 [0.2–18.9]	<b>P = .007</b>
Hypoechoic	8.14 $\pm$ 5.76	8.15 [0–31]	
Posterior features			Z = 2.385
No shadowing	6.69 $\pm$ 5.87	4.7 [0–31]	<b>P = .017</b>
Shadowing	8.65 $\pm$ 4.87	9.3 [0.7–25.9]	

Bold values indicate statistically significant difference.



circumscribed, while 31 (62%) of malignant lesions had spiculated margins. Homogeneous contrast enhancement was observed in 48 (77.4%) benign lesions, whereas heterogeneous contrast enhancement was observed in 44 (88%) malignant lesions. In dynamic breast MRI, 46 (74.2%) benign masses showed a type 1 (persistent) kinetic curve. Eight benign lesions displayed a type 3 (washout) kinetic curve. Among malignant masses, 32 (64%) had a type 3 kinetic curve, while 10 (20%) had a type 1 kinetic curve.

### Diagnostic Performances of US, SMI, and MRI

In our study, when BI-RADS 1, 2, and 3 lesions were classified as benign, and BI-RADS 4a, 4b, 4c, and 5 lesions were classified as malignant, the sensitivity was 86%, specificity was 64.38%, PPV was 62.3%, NPV was 83.7%, and accuracy was 70.5%.

The VI index value had a statistically significant effect on distinguishing between histopathologically benign and malignant lesions in our study. The area under the curve (AUC) value was 0.79 according to ROC analysis ( $P < .001$ ), indicating a high diagnostic value of discrimination. The cut-off value of the VI index was calculated as 4.15 according to Youden's index, and the AUC value of 0.76 was statistically significant according to ROC analysis ( $P < .001$ ). At the cut-off value of 4.15, the sensitivity, specificity, PPV, NPV, and accuracy of the VI were calculated as 92, 60, 64.8, 90.2, and 74%, respectively (Table 6).

When BI-RADS categories 1, 2, and 3 were considered benign and BI-RADS categories 4 and 5 were considered malignant, the diagnostic performance of dynamic breast MRI yielded sensitivity, specificity, PPV, NPV, and accuracy of 98, 80.65, 80.3, 98, and 88.39%, respectively.

Our study demonstrated that US, VI, and MRI significantly contributed to differentiating between histopathologically benign and malignant lesions, as evidenced by AUC values of 0.71, 0.76, and 0.89, respectively, in the ROC analysis ( $P < .001$ ). These AUC values suggest a moderate to strong level of discriminatory power (Figure 4).

## Discussion

In this study, we evaluated the diagnostic accuracy of SMI and DCE MRI in distinguishing between benign and malignant breast masses. Our results indicated that SMI, with VI cut-off value of 4.15, achieved a sensitivity of 92%, specificity of 60%, and accuracy of 74%. These findings suggest that SMI can effectively differentiate between benign and malignant lesions based on their microvascular characteristics, providing a valuable adjunct to conventional imaging modalities.

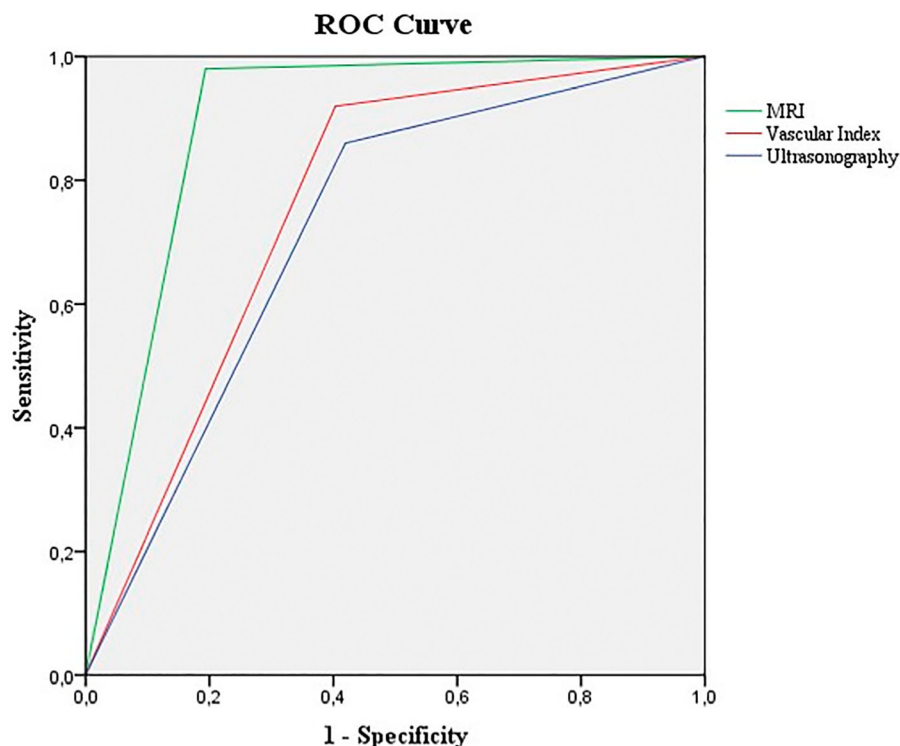
In the literature, VI cutoff values have been reported to range from 1.1 to 8.9, with most studies identifying a cutoff around 4, which closely aligns with the cutoff value determined in our study. The reported sensitivity, specificity, and accuracy for VI range from 70.2 to 99%, 41 to 91.2%, and 66.9 to 88.6%, respectively.<sup>11,15–24</sup> However, several factors may contribute to variations in VI measurements. First, the compression applied during ultrasound imaging can influence the visibility of microvascular structures. Additionally, both ultrasound and SMI are highly dependent on the operator's skill and patient factors, which can lead to inconsistencies. Nevertheless, the sensitivity, specificity, and accuracy in our study are consistent with previously reported values.

**Table 6.** The Relationship Between Vascular Index (VI) and the Cutoff Value Was Evaluated in Correlation with Histopathological Results

		AUC	P-Value	95% Confidence Interval
Vascular index		0.79	<b>&lt;0.001</b>	0.707–0.875
VI cutoff value		0.76	<b>&lt;0.001</b>	0.668–0.849
		Malign	Benign	Sensitivity 92%
				Specificity 60%
				PPV 64.80%
				NPV 90.20%
VI cutoff value	>4.15	46	25	Accuracy 74%
	≤4.15	4	37	

Bold values indicate statistically significant difference.

**Figure 4.** Receiver operating characteristic (ROC) curves are shown to differentiate between malignant and benign breast masses across various imaging modalities, including magnetic resonance imaging (MRI), vascular imaging (VI), and ultrasonography (US).



In previous studies, the effectiveness of techniques such as SMI, CDUS, PDUS, contrast-enhanced ultrasound, and elastography in differentiating benign from malignant breast lesions has been demonstrated.<sup>7,11,18,19,25,26</sup> Therefore, our study is unique as it represents the first to directly compare the efficacy of SMI with DCE breast MRI in distinguishing between benign and malignant lesions. Our analysis showed that higher VI values were associated with increased washout, as seen with type 3 kinetic contrast enhancement curves, which are typically indicative of malignancy. This finding suggests a positive correlation between higher VI values and malignant lesions. In benign lesions with type 1 kinetic curves and those without enhancement, the mean VI values were 5.13 and 1, respectively. When these groups were combined, the mean VI value was 4.85, which aligns closely with the VI cutoff value we established. We believe that the slightly elevated VI mean in lesions with type 1 curves, relative to our cutoff, could be due to the presence of lesions that,

despite showing type 1 curves, were histopathologically malignant.

Tekinhatur et al.<sup>27</sup> conducted a study with 120 breast lesions, comparing the diagnostic effectiveness of contrast-enhanced mammography and DCE breast MRI. The study suggested that contrast-enhanced mammography could serve as an alternative to DCE breast MRI. Similarly, our study indicates that the SMI could be a viable alternative imaging technique in settings where MRI is unavailable. Given the practicality of both contrast-enhanced mammography and SMI, we anticipate that these methods will become increasingly important in the future.

Despite the significant findings, this study has several limitations. Initially, the limited sample size could limit the extent to which the findings can be generalized to a broader population. Secondly, the study was conducted at a single center, which could introduce selection bias. Additionally, the VI measurements were performed by a single operator, highlighting a limitation related to operator dependency. This

dependence on a single operator for SMI measurements may lead to measurement bias. Future research should aim to include larger, multicenter cohorts with standardized protocols to further validate and expand upon our findings.

In conclusion, our study demonstrates that SMI, when used alongside conventional imaging modalities such as grayscale US and DCE MRI, offers significant benefits in distinguishing benign from malignant breast masses. The clinical implications are substantial, suggesting that SMI could be integrated into routine breast cancer screening and diagnostic workflows to enhance early detection and treatment planning. These findings underscore the importance of a multimodal imaging approach, combining the strengths of SMI and MRI to achieve optimal diagnostic accuracy in breast cancer evaluation.

## Data Availability Statement

Research data are not shared.

## References

1. Ferlay JEM, Lam F, Laversanne M, et al. *Global Cancer Observatory: Cancer Today*. Lyon, France: International Agency for Research on Cancer; 2024. <https://gco.iarc.who.int/today>. Accessed August 6, 2024.
2. Mann RM, Hooley R, Barr RG, Moy L. Novel approaches to screening for breast cancer. *Radiology* 2020; 297:266–285.
3. Giaquinto AN, Sung H, Newman LA, et al. Breast cancer statistics 2024. *CA Cancer J Clin* 2024; 74:477–495.
4. Sardanelli F, Magni V, Rossini G, Kilburn-Toppin F, Healy NA, Gilbert FJ. The paradox of MRI for breast cancer screening: high-risk and dense breasts-available evidence and current practice. *Insights Imaging* 2024; 15:96.
5. Kuhl CK. MRI of breast tumors. *Eur Radiol* 2000; 10:46–58.
6. Blood CH, Zetter BR. Tumor interactions with the vasculature: angiogenesis and tumor metastasis. *Biochim Biophys Acta* 1990; 1032:89–118.
7. Xiao XY, Chen X, Guan XF, Wu H, Qin W, Luo BM. Superb microvascular imaging in diagnosis of breast lesions: a comparative study with contrast-enhanced ultrasonographic microvascular imaging. *Br J Radiol* 2016; 89:20160546.
8. Zhan J, Diao XH, Jin JM, Chen L, Chen Y. Superb microvascular imaging—a new vascular detecting ultrasonographic technique for avascular breast masses: a preliminary study. *Eur J Radiol* 2016; 85:915–921.
9. Aziz MU, Eisenbrey JR, Deganello A, et al. Microvascular flow imaging: a state-of-the-art review of clinical use and promise. *Radiology* 2022; 305:250–264.
10. Ferda J, Frolich M, Ferdova E, Heidenreich F, Charvat R, Mirka H. Neovascularization, vascular mimicry and molecular exchange: the imaging of tumorous tissue aggressiveness based on tissue perfusion. *Eur J Radiol* 2023; 163:110797.
11. Chae EY, Yoon GY, Cha JH, Shin HJ, Choi WJ, Kim HH. Added value of the vascular index on superb microvascular imaging for the evaluation of breast masses: comparison with grayscale ultrasound. *J Ultrasound Med* 2021; 40:715–723.
12. Aslan HS, Arslan M, Alver KH, Vurgun S, Demirci M, Tekinhatun M. Role of superb microvascular imaging (SMI) vascularity index values and vascularity patterns in the differential diagnosis of malignant liver lesions. *Abdom Radiol (NY)* 2024; 1–14.
13. Kuhl CK, Mielcareck P, Klaschik S, et al. Dynamic breast MR imaging: are signal intensity time course data useful for differential diagnosis of enhancing lesions? *Radiology* 1999; 211:101–110.
14. El Khoul RH, Macura KJ, Jacobs MA, et al. Dynamic contrast-enhanced MRI of the breast: quantitative method for kinetic curve type assessment. *AJR Am J Roentgenol* 2009; 193:W295–W300.
15. Park AY, Kwon M, Woo OH, et al. A prospective study on the value of ultrasound microflow assessment to distinguish malignant from benign solid breast masses: association between ultrasound parameters and histologic microvessel densities. *Korean J Radiol* 2019; 20:759–772.
16. Cai SM, Wang HY, Zhang XY, et al. The vascular index of superb microvascular imaging can improve the diagnostic accuracy for breast imaging reporting and data system category 4 breast lesions. *Cancer Manag Res* 2020; 12:1819–1826.
17. Cai S, Wang H, Zhang X, et al. Superb microvascular imaging technology can improve the diagnostic efficiency of the BI-RADS system. *Front Oncol* 2021; 11:634752.
18. Lee EJ, Chang YW. Combination of quantitative parameters of shear wave elastography and superb microvascular imaging to evaluate breast masses. *Korean J Radiol* 2020; 21:1045–1054.
19. Uysal E, Ozturk M, Kilincer A, Koplay M. Comparison of the effectiveness of shear wave elastography and superb microvascular imaging in the evaluation of breast masses. *Ultrasound Q* 2021; 37:191–197.
20. Lee EJ, Chang YW. Prospective analysis of breast masses using the combined score for quantitative ultrasonography parameters. *Sci Rep* 2022; 12:16205.
21. Arslan FZ, Altunkeser A, Korez MK, Aksoy N, Bayramoglu Z, Karagulle M. The importance of superb microvascular imaging for the differentiation of malignant breast lesions from benign lesions. *Eur J Breast Health* 2022; 18:48–54.
22. Lee EJ, Chang YW, Oh E, Hwang J, Kim HJ, Hong SS. Reproducibility and diagnostic performance of the vascular index of superb

- microvascular imaging in real-time breast ultrasonography for evaluating breast masses. *Ultrasonography* 2021; 40:398–406.
23. Zhang XY, Zhang L, Li N, et al. Vascular index measured by smart 3-D superb microvascular imaging can help to differentiate malignant and benign breast lesion. *Cancer Manag Res* 2019; 11:5481–5487.
24. Chen SH, Xiang XZ, Che PF, et al. Superb microvascular imaging for the differentiation of benign and malignant breast lesions: a system review and meta-analysis. *J Ultrasound Med* 2023; 42:1385–1399.
25. Kayadibi Y, Bulut IN, Aladag Kurt S, et al. The role of superb microvascular imaging and shearwave elastography in the evaluation of intraductal papilloma-like lesions. *J Ultrasound Med* 2022; 41:995–1008.
26. Ma Y, Li G, Li J, Ren WD. The diagnostic value of superb microvascular imaging (SMI) in detecting blood flow signals of breast lesions: a preliminary study comparing SMI to color Doppler flow imaging. *Medicine (Baltimore)* 2015; 94:e1502.
27. Tekinhatun M, Sabir N, Erdem E, Yilmaz S, Ufuk F. Dynamic contrast-enhanced mammography and breast MRI in the diagnosis of breast cancer and detection of tumor size. *Turk J Med Sci* 2024; 54:249–261.